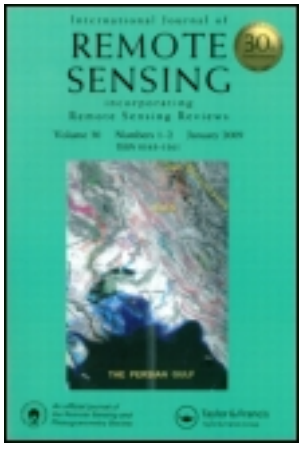

International Journal of Remote Sensing

Publication details, including instructions for authors and subscription information:
http://www.tandfonline.com/loi/tres20

Super-resolution mapping using Hopfield Neural Network with panchromatic imagery

Quang Minh Nguyen [a] , Peter M. Atkinson [b] & Hugh G. Lewis [b]

[a] Faculty of Surveying and Mapping, Hanoi University of Mining and Geology, Hanoi, Vietnam

[b] Graduate School of Geography, University of Southampton, Southampton, SO17 1BJ, UK

Available online: 12 Jul 2011

To cite this article: Quang Minh Nguyen, Peter M. Atkinson & Hugh G. Lewis (2011): Super-resolution mapping using Hopfield Neural Network with panchromatic imagery, International Journal of Remote Sensing, 32:21, 6149-6176

To link to this article: http://dx.doi.org/10.1080/01431161.2010.507797

International Journal of Remote Sensing
Vol. 32, No. 21, 10 November 2011, 6149–6176

Taylor & Francis
Taylor & Francis Group

Super-resolution mapping using Hopfield Neural Network with panchromatic imagery

QUANG MINH NGUYEN*†, PETER M. ATKINSON‡ and HUGH G. LEWIS‡
†Faculty of Surveying and Mapping, Hanoi University of Mining and Geology, Hanoi, Vietnam
‡Graduate School of Geography, University of Southampton, Southampton SO17 1BJ, UK

(*Received 11 March 2010; in final form 2 July 2010*)

Land-cover proportions of mixed pixels can be predicted using soft classification. From the land-cover proportions, a hard land-cover map can be predicted at sub-pixel spatial resolution using super-resolution mapping techniques. It has been demonstrated that the Hopfield Neural Network (HNN) provides a suitable method for super-resolution mapping. To increase the detail and accuracy of the sub-pixel land-cover map, supplementary information at an intermediate spatial resolution can be used. In this research, panchromatic (PAN) imagery was used as an additional source of information for super-resolution mapping. Information from the PAN image was captured by a new PAN reflectance constraint in the energy function of the HNN. The value of the new PAN reflectance constraint was defined based on forward and inverse models with local end-member spectra and local convolution weighting factors. Two sets of simulated and degraded data were used to test the new technique. The results indicate that PAN imagery can be used as a source of supplementary information to increase the detail and accuracy of sub-pixel land-cover maps produced by super-resolution mapping from land-cover proportion images.

1. Introduction

In practice, the nature of the real landscape and the data-acquisition process cause many 'mixed pixels' in remotely sensed images (Schowengerdt 1997). Using hard-classification approaches, thematic maps can be obtained at the image spatial resolution in which each pixel is assigned to just one class (Foody 2004). In such approaches, a mixed pixel is normally classified to a land-cover class if the probability of the mixed pixel belonging to that class is the greatest. In hard classification, it is obvious that some information is lost given the existence of other classes in the mixed pixels.

Soft-classification approaches predict the proportion of each land-cover class within each pixel. Several soft-classification approaches have been introduced, including spectral mixture modelling (Settle and Drake 1993), fuzzy *c*-means classifiers (Bastin 1997), *k*-nearest neighbour classifiers (*k*-NN) (Schowengerdt 1996), artificial neural networks (Foody *et al.* 1997, Carpenter *et al.* 1999) and support vector machines (Brown *et al.* 2000). Using soft classification, a land-cover map can be represented

*Corresponding author. Email: ng.q.minh@gmail.com

International Journal of Remote Sensing
ISSN 0143-1161 print/ISSN 1366-5901 online © 2011 Taylor & Francis
http://www.tandf.co.uk/journals
http://dx.doi.org/10.1080/01431161.2010.507797

by a set of proportion images in which the value of each pixel is the proportion for a land-cover class. These images are more informative and appropriate depictions of land cover than conventional hard-classified maps. However, there still exists uncertainty because the location of the land-cover classes in the mixed pixels remains unknown.

Super-resolution mapping is a set of techniques for predicting the location of land-cover classes within a pixel based on the proportion images. In comparison with the land-cover maps obtained from conventional hard classification, the maps resulting from super-resolution classification are more detailed and accurate (Atkinson 1997, Tatem *et al.* 2001a, 2001b, 2002). Super-resolution mapping techniques are based on the assumption that a pixel can be represented as a matrix of sub-pixels. Each sub-pixel belongs to a land-cover class, and the number of sub-pixels of each class is specified by the soft-classified land-cover proportions. The location of these sub-pixels can be predicted based on the concept of spatial dependence, which refers to the tendency of proximate sub-pixels to be more alike than those located far apart. Based on the phenomenon of spatial dependence, several techniques have been proposed for super-resolution mapping: spatial dependence maximization (Atkinson 1997), sub-pixel per-field classification (Aplin and Atkinson 2001), linear optimization techniques (Verhoeye and De Wulf 2002), Hopfield Neural Network (HNN) optimization (Tatem *et al.* 2001a, 2001b, 2002), two-point histogram optimization (Atkinson 2008), genetic algorithms (Mertens *et al.* 2003) and feed-forward neural networks (Mertens *et al.* 2004, Zhang *et al.* 2008). In spite of presenting improvements in comparison with conventional hard classification, these super-resolution mapping methods are limited in terms of the detail and accuracy of the resulting thematic map, since they are based only on the soft-classified proportions at the pixel level and the assumption of spatial dependence. It is, therefore, suggested that information available at a finer spatial resolution could be used to increase the detail and accuracy of the sub-pixel land-cover map resulting from super-resolution classification (Nguyen *et al.* 2005). Several sources of information at a finer resolution have been used for super-resolution mapping such as geo-statistical data (Boucher and Kyriakidis 2006), fused images (Nguyen *et al.* 2006) and panchromatic (PAN) imagery (Atkinson 2008).

Several remote-sensing systems provide both multispectral (MS) and PAN sensors such as Satellite Pour l 'Observation de la Terre (SPOT) 5 (with 10 m MS and 5 m PAN imagery), IKONOS (4 m MS and 1 m PAN imagery) or QuickBird (2.6 m MS and 0.6 m PAN imagery). In the same remote-sensing system, the MS images usually have a coarser spatial resolution but finer spectral resolution. For land-cover classification, MS imagery is commonly used because of its fine spectral resolution. PAN imagery, although with finer spatial resolution, is rarely used for land-cover classification because of its coarse spectral resolution. However, for super-resolution mapping, the fine spatial resolution PAN image can provide useful information for producing more detailed and accurate sub-pixel land-cover maps at a spatial resolution that is finer than either MS or PAN input images.

2. Method

The new method proposed in this article aims to use a PAN image as additional information for super-resolution mapping. To make use of the PAN image for land-cover mapping, a forward model, a spectral convolution model and an inverse model were employed in the form of a PAN reflectance constraint within an established

super-resolution mapping method (HNN optimization). The PAN reflectance constraint was obtained using a rule of minimum grey value difference between synthetic and the real PAN image.

Figure 1 is a graphical depiction of the method proposed for incorporating a PAN image into super-resolution mapping using a HNN. From the MS images at the original spatial resolution, the set of land-cover area proportion images is produced using a soft classifier. The proportion images are then used to produce the sub-pixel land-cover class at the first iteration using the HNN (each sub-pixel is represented by a neuron in the HNN). From the super-resolution map at the first iteration, an estimated MS image (at the PAN image spatial resolution) is then produced using a forward model and spatial convolution. The estimated MS image is then convolved spectrally to create a synthetic PAN image. By comparing the observed and synthetic PAN images, a value is produced for all neurons covered by the same pixel in the PAN image to make the synthetic PAN converge to the observed PAN image. Thus the HNN is constrained by the grey values of the observed PAN image. The adjustment value, or PAN reflectance constraint value, along with the goal and constraint values in the HNN structure proposed by Tatem *et al.* (2001b), can be used in the optimization process for super-resolution mapping by minimizing the energy function. After the optimization process, the estimated grey value of the synthetic PAN image produced from sub-pixels in the super-resolution land-cover map should be similar to the observed PAN image.

The method presented is based on the structure of the HNN proposed by Tatem *et al.* (2001b). The structure of the HNN for super-resolution mapping of two land-cover classes can be seen in figure 2. A pixel at the original spatial resolution is divided into two interconnected matrices of neurons in the HNN. Each neuron (h, i, j)

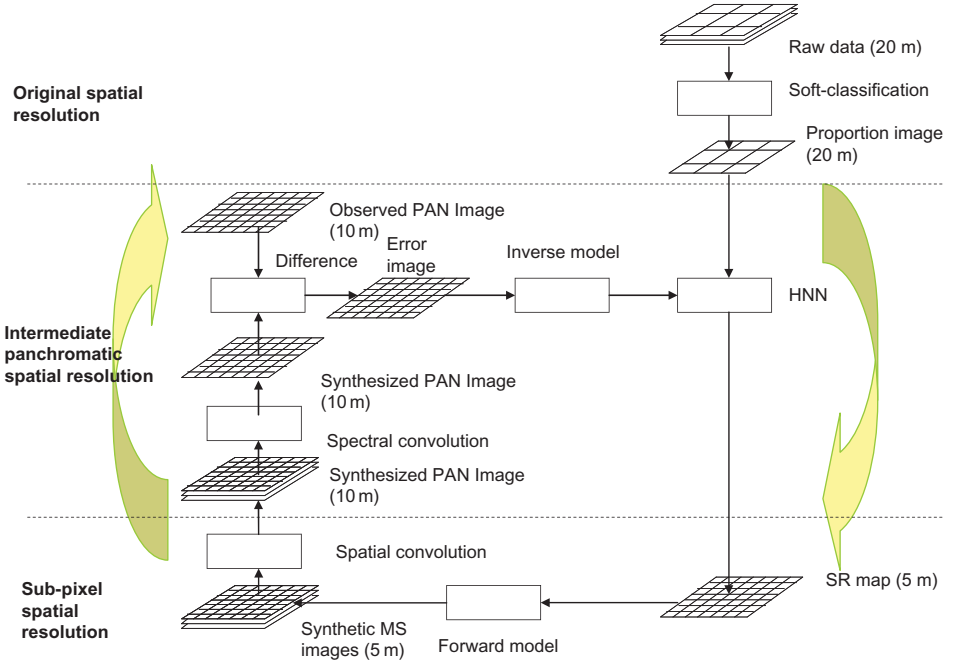

Figure 1. HNN super-resolution mapping using a PAN image.

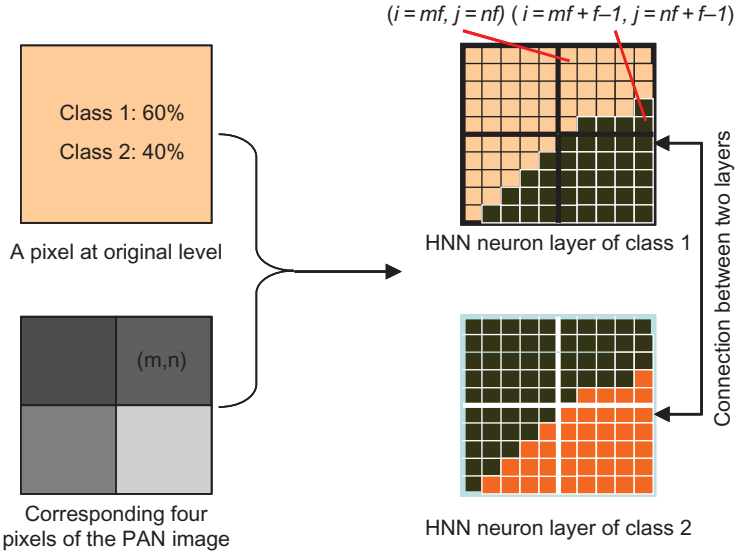

Figure 2. PAN reflectance constraint for sub-pixels covered by pixel (m, n) at the PAN spatial resolution. A pixel at the original level contains 4 pixels at the PAN image resolution, and each pixel in the PAN image contains $f \times f$ sub-pixels. m, n are the coordinates of the PAN pixel. The PAN reflectance constraint ensures that the grey value of the pixel (m, n) of the synthetic PAN image estimated from the neuron output is as close as possible to the grey value of the corresponding pixel of the observed PAN image.

represents a sub-pixel at position (i, j) in the land-cover class h, and each matrix of neurons represents a land-cover class. For super-resolution mapping, the HNN is initialized using the soft-classified land-cover proportions and runs until it converges to a monotonic stable state when the energy function is minimized. At the stable state, the output values of the neurons are binary values. If the output value of the neuron (h, i, j) is 1, the sub-pixel (i, j) is assigned to the land-cover class h. Otherwise, if the output value is 0, the sub-pixel (i, j) does not belong to the class h. The energy function can be expressed as

$$E = -\sum_{h}\sum_{i}\sum_{j}(k_1 G1_{hij} + k_2 G2_{hij} + k_3 P_{hij} + k_4 M_{hij}), \tag{1}$$

where k_1, k_2, k_3 and k_4 are weighting constants. The weighting constants determine the effects of the goal functions $G1_{hij}$ and $G2_{hij}$, proportion constraint P_{hij} and multi-class constraint M_{hij} to the energy function. The optimal values of the weighting constants are determined empirically for super-resolution mapping (Tatem *et al.* 2002).

For each neuron (h, i, j), the values of spatial clustering or goal functions $G1_{hij}$ and $G2_{hij}$ can be determined by

$$\frac{\mathrm{d}G1_{hij}}{\mathrm{d}v_{hij}} = \frac{1}{2}\left[1 + \tanh\left(\frac{1}{8}\sum_{\substack{d=i-1\\ d\neq i}}^{i+1}\sum_{\substack{e=i-1\\ e\neq j}}^{j+1} v_{hde} - 0.5\right)\lambda\right](v_{hij} - 1) \tag{2}$$

and

$$\frac{\mathrm{d}G2_{hij}}{\mathrm{d}v_{hij}} = \frac{1}{2}\left\{1 + \left[-\tanh\left(\frac{1}{8}\sum_{\substack{d=i-1\\d\neq i}}^{i+1}\sum_{\substack{e=i-1\\e\neq j}}^{j+1} v_{hde} - 0.5\right)\lambda\right]\right\}(v_{hij}), \tag{3}$$

where λ is the gain value that is usually assigned a value of 100, 0.5 is the threshold to allocate a neuron to land-cover class h and $1/8 \equiv 1/N$, where N is the number of neighbouring sub-pixels used in the goal function. The first goal function (equation (2)) is used to increase the output value v_{hij} of the neuron if the average output value of the eight surrounding neurons is >0.5. In contrast, the second goal function (equation (3)) decreases v_{hij} if the average output value of the eight surrounding neurons is <0.5.

The land-cover proportion for each original pixel is retained by the proportion constraint value P_{hij} in equation (1) as

$$\frac{\mathrm{d}P_{hij}}{dv_{hij}} = \frac{1}{2z^2}\sum_{d=xz}^{xz+z-1}\sum_{e=yz}^{yz+z-1}[1 + \tanh(v_{hde} - 0.5)\lambda] - a_{hxy}, \tag{4}$$

where $\frac{1}{2z^2}\sum_{d=xz}^{xz+z-1}\sum_{e=yz}^{yz+z-1}[1 + \tanh(v_{hde} - 0.5)\lambda] - a_{hxy}$ is the estimated proportion and a_{hxy} is the input proportion of the land cover h of the pixel (x, y), which is obtained by soft classification. The pixel (x, y) is defined at the original spatial resolution and covers the sub-pixel or neuron (h, i, j). The zoom factor z determines the increase in spatial resolution from the original image to the super-resolution mapping image. The proportion constraint function value is positive if the estimated proportion of the class h is greater than the input proportion. As a result, the network reduces the output values of neurons in the class layer h. Conversely, if the estimated proportion is less than the input proportion, the proportion constraint produces a negative value to increase the output values of the neurons in class h.

The multi-class value M_{hij} is used to reduce the output of the neurons if the sum of outputs of c classes at the position (i, j) is >1. If the sum of outputs of c classes is <1, the function increases the output of the neurons at the position (i, j). The value of the multi-class constraint is calculated as

$$\frac{\mathrm{d}M_{hij}}{\mathrm{d}v_{hij}} = \left(\sum_{k=1}^{c} v_{kij}\right) - 1. \tag{5}$$

To use the PAN image for super-resolution mapping, a PAN reflectance constraint is added to the energy function in equation (1). The new energy function can be expressed as follows

$$E = -\sum_{h}\sum_{i}\sum_{j}(k_1 G1_{hij} + k_2 G2_{hij} + k_3 P_{hij} + k_4 M_{hij} + k_5 R^P_{hij}), \tag{6}$$

where R^P_{hij} is the PAN reflectance constraint value for each neuron (h, i, j).

The structure of the modified HNN can be seen in figure 2. Each neuron in the HNN represents a sub-pixel in the original spatial resolution image. The factor f determines

the increase in spatial resolution of the new super-resolution image in comparison with the PAN image. Apart from the proportion constraint for each original pixel, $f \times f$ sub-pixels covered by pixel (m, n) of the PAN images are constrained by a PAN reflectance constraint. The reflectance constraint is based on the principle that the estimated grey value of a pixel of the PAN image should be equal to the grey value of that pixel in the observed PAN image.

The new energy function in equation (6) is minimized if the derivatives of variables in equation (6) converge to 0 for each neuron (h, i, j),

$$\frac{\mathrm{d}E_{hij}}{\mathrm{d}v_{hij}} = k_1 \frac{\mathrm{d}G1_{hij}}{\mathrm{d}v_{hij}} + k_2 \frac{\mathrm{d}G2_{hij}}{\mathrm{d}v_{hij}} + k_3 \frac{\mathrm{d}P_{hij}}{\mathrm{d}v_{hij}} + k_4 \frac{\mathrm{d}M_{hij}}{\mathrm{d}v_{hij}} + k_5 \frac{\mathrm{d}R_{hij}}{\mathrm{d}v_{hij}}. \tag{7}$$

The derivative values of $G1$, $G2$, P and M with respect to v_{hij} are computed by equations (2)–(5), respectively. The value $\mathrm{d}R_{hij}/\mathrm{d}v_{hij}$ is derived based on the forward and inverse models, spatial and spectral convolutions as in figure 1.

2.1 *Forward model*

The forward model is used to estimate a set of MS bands from a land-cover image. The estimated reflectance of the neurons representing the pixel (m, n) of b MS bands at the PAN spatial resolution can be defined by a forward model as

$$\begin{aligned} R^t_{B1} &= S_{B1,1} V_{C1} + \ldots + S_{B1,c} V_{Cc} \\ R^t_{B2} &= S_{B2,1} V_{C1} + \ldots + S_{B2,c} V_{Cc} \quad \text{or } R^t = \mathbf{S}\boldsymbol{V}^t, \\ R^t_{B3} &= S_{B3,1} V_{C1} + \ldots + S_{B3,c} V_{Cc} \end{aligned} \tag{8}$$

where the estimated proportion value of a class i at the time t is $V^t_{Ci} = 1/f^2 \left(\sum_{p=mf}^{mf+f-1} \sum_{q=nf}^{nf+f-1} v_{ipq} \right)$, s_{BiCj} is the spectral value of the land-cover class j for a spectral band Bi, $\boldsymbol{R}^t_{m,n} = [R^t_{B1}, R^t_{B2}, \ldots, R^t_{Bb}]^T_{mn}$, $\mathbf{V}^t_{m,n} = [V^t_{C1}, V^t_{C2}, \ldots, V^t_{Cb}]^t_{mn}$ and

$$\mathbf{S} = \begin{bmatrix} s_{B1C1} & \ldots & s_{B1Cc} \\ s_{B2C1} & \ldots & s_{B2Cc} \\ s_{BbC1} & \ldots & s_{BbCc} \end{bmatrix}. \tag{9}$$

2.2 *Spectral convolution*

The spectral convolution procedure is employed to create a synthetic PAN image from a set of MS bands. Spectral convolution can be based on the synthesising method proposed by Zhang (1999) as

$$R_{\mathrm{Pan}} = \sum_i \varphi_i R_{Bi}, \tag{10}$$

where R_{Pan} is the digital value of the synthetic PAN image, R_{Bi} is the reflectance value of the MS band i and φ_i is a weighting factor for the MS band i. The weight factor φ_i can be calculated directly from the degraded MS and images at the original spatial resolution.

2.3 *Error image*

From the observed PAN image, it is possible to produce an error image that can be used for HNN super-resolution mapping. The error image is the difference between the observed PAN image and the synthetic PAN image created by the neuron output of the HNN at time t. The error image can be calculated as

$$E = R^{\mathrm{o}} - R^{t}_{\mathrm{PanSyn}}, \tag{11}$$

where R° is the observed PAN image and R^{t}_{PanSyn} is the synthetic PAN image at the time t, which can be calculated by the spectral convolution model (equation (10)) as

$$R^{t}_{\mathrm{PanSyn}} = \sum \varphi_i R^{t}_{Bi}. \tag{12}$$

2.4 *Inverse model and PAN reflectance constraint*

From the error image, an output value for each neuron in the HNN can be produced based on an inverse model. This output value can be named the PAN reflectance constraint, which is used to retain the grey value of each pixel of the PAN image. If the grey value of a synthesized PAN pixel is greater than that of the corresponding observed PAN pixel, the constraint produces a value to reduce the value of the synthetic image. Conversely, if the synthetic reflectance value of a PAN pixel is smaller than that of the observed PAN image, the constraint produces a value to increase the value of the synthetic image.

Suppose that the MS bands at spatial resolution of PAN image are $B_1, B_2, \ldots, B_b$ and the estimated land-cover proportions of c land-cover classes for pixel (m, n) are $P_1, P_2, \ldots, P_c$. Using the forward model in equation (8), the relationship between the reflectance of the MS bands and the land-cover classes can be expressed as

$$\begin{aligned} R^{\mathrm{o}}_{B1} &= S_{B1,1}P_1 + \ldots + S_{B1,c}P_C \\ R^{\mathrm{o}}_{B2} &= S_{B2,1}P_1 + \ldots + S_{B2,c}P_C \\ R^{\mathrm{o}}_{B3} &= S_{Bb,1}P_1 + \ldots + S_{Bb,c}P_C \end{aligned} \quad \text{or } \boldsymbol{R}^{\mathrm{o}}_{mn} = \boldsymbol{S}\boldsymbol{P}_{mn}, \tag{13}$$

where $\boldsymbol{R}_{mn} = [R_{B1} \ldots R_{Bi} \ldots R_{Bb}]^T_{mn}$ is the vector of reflectance values of the bands $B_1, \ldots, B_{\mathrm{i}}, \ldots, B_{\mathrm{b}}$ and $\boldsymbol{P}_{mn} = [P_1 \ldots P_2 \ldots P_c]^T_{mn}$ is the vector of land-cover proportion values. In sub-pixel mapping, based on the assumption that a pixel consists of a matrix of crisp sub-pixels, the land-cover proportions $P_1, P_2, \ldots, P_c$ must be a whole number of sub-pixels. For example, if a pixel in the PAN image consists of 2×2 sub-pixels, the land-cover proportion P_i of a given land-cover class should be selected from the integer values 0, 1, 2, 3 and 4 and divided by 4. The land-cover proportions of all c land-cover classes of a pixel in the PAN image are a combination of integer values such as $P_1 = 1, \ldots, P_i = 0, \ldots, P_c = 3$ divided by 4, with $P_1 + P_2 + \ldots + P_c = 1$. The synthetic grey value of a PAN pixel converges to the observed grey value when the estimated proportion value V^{t}_{Ci} of class c_i at time t is equal to the observed land-cover proportion P_i.

The land-cover class proportions for each PAN pixel can be determined from a limited number of possible *combinations* of land-cover class. For example, land-cover proportions of a PAN pixel (m, n), which contains two land-cover classes P_1 and P_2, can be one of the possible *combinations* (provided that a pixel in the PAN image covers 2×2 sub-pixels) such as [$P_1 = 0/4$, $P_2 = 4/4$], [$P_1 = 1/4$, $P_2 = 3/4$], [$P_1 = 2/4$, $P_2 = 2/4$], [$P_1 = 3/4$, $P_2 = 1/4$] or [$P_1 = 4/4$, $P_2 = 0/4$] and only one of them is correct. In this research, the correct land-cover proportion combination within a PAN pixel was determined based on the minimum grey value difference method.

The minimum grey value difference method is based on the forward model (equation (8)) and spectral convolution (equation (10)). To calculate the land-cover proportions for pixel (m, n) in the PAN image, the difference between the synthetic grey value computed from each possible land-cover proportion combination and the observed grey value is calculated. The land-cover proportion combination of the pixel is then chosen based on the minimum difference. The process can be expressed by a rule as follows:

$$\boldsymbol{P} = \boldsymbol{P}_i \text{ if } (|R_i^{\text{Synthetic}} - R^{\text{Observed}}|_{mn} = \min), \tag{14}$$

where $\boldsymbol{P}$ is a vector of land-cover proportions for PAN pixel (m, n), $\boldsymbol{P}_i$ is the vector of land-cover proportions for combination i, $R_i^{\text{Synthetic}}$ is synthetic grey value for the land-cover proportion combination i and R^{observed} is the grey value of the observed PAN image. When the land-cover proportion image $\boldsymbol{P}$ is obtained, the PAN reflectance function value can be calculated as

$$\mathrm{d}R/\mathrm{d}v_{hij} = P_{hmn} - V_{hmn}^t, \tag{15}$$

where (m, n) is the corresponding MS pixel of the PAN pixel (i, j), P_{hmn} is the land-cover proportion of class h and V_{hmn}^t is the estimated land-cover proportion of class h of the MS pixel (m, n) at time t.

Using the PAN reflectance constraint, the land-cover proportions produced from all pixels of the PAN image covered by a pixel (x, y) of the original image should be close to the land-cover proportions of the pixel (x, y) predicted by soft classification. To ensure that, an empirical weighting mechanism was used to adjust the weighting constant k_5 in equation (7) as

$$\text{If } [(\boldsymbol{P}_{\text{PAN}}^{xy} - \boldsymbol{P}_{\text{Soft-classified}}^{xy})] > 0.2] \text{ then } (k_5 = k_5/10). \tag{16}$$

where $\boldsymbol{P}_{\text{PAN}}^{xy}$ is the land-cover proportion produced from all pixels of the PAN image located within the pixel (x, y) and $\boldsymbol{P}_{\text{Soft-classified}}^{xy}$ is the land-cover proportion predicted by soft classification.

3. Example 1: simulated IKONOS image

3.1 *Data*

Prior to application to real data, the proposed method was tested using a set of simulated images used previously in Nguyen *et al.* (2006). In this data set, a 32 m MS image and an 8 m PAN image were simulated using a real IKONOS image. The ratio between the spatial resolutions of the simulated MS and PAN image is similar to the ratio

between the real 4 m MS and 1 m PAN IKONOS image. Thus the algorithm should be applicable to the real images if it performs well on the simulated images. The simulation ensured that there were no errors in image registration between the reference image and the land-cover image obtained by super-resolution mapping. Therefore, the evaluation focused on the performance of the algorithm itself.

The simulation data set included 32 m MS (figure 3(*a*)–(*d*)) and 8 m (figure (3(*e*)) PAN images generated from 4 m reference cereal, grass and trees classes (figure 4(*a*)–(*d*)) using random normal distributions based on the means and variances of each class in the MS bands. The means and variances of three land-cover classes in each MS band were obtained through an analysis of reference land-cover classes and a real IKONOS image. The 32 m land-cover proportion images (figure 5(*a*)–(*c*)) were produced by k-NN soft classification with $k = 5$ (Schowengerdt 1996) applied to the simulated 32 m MS images. The obtained land-cover proportion images contained an amount of error similar to that which can be obtained from the real data, with an overall area error proportion of 0.56% and an overall root mean square (RMS) error of 0.084 pixels (Tatem *et al.* 2001b).

3.2 *Local end-member spectra*

Investigation of the real IKONOS image indicated that the end-member spectra of the same class in adjacent pixels were similar while the end-member spectra of more distant pixels were different. Thus a single set of global end-member spectra values used in equation (2) was not appropriate for every pixel in the image. Local end-member spectra were deemed more appropriate for determining a local reflectance constraint value. Local end-member spectra can be produced from the land-cover proportion

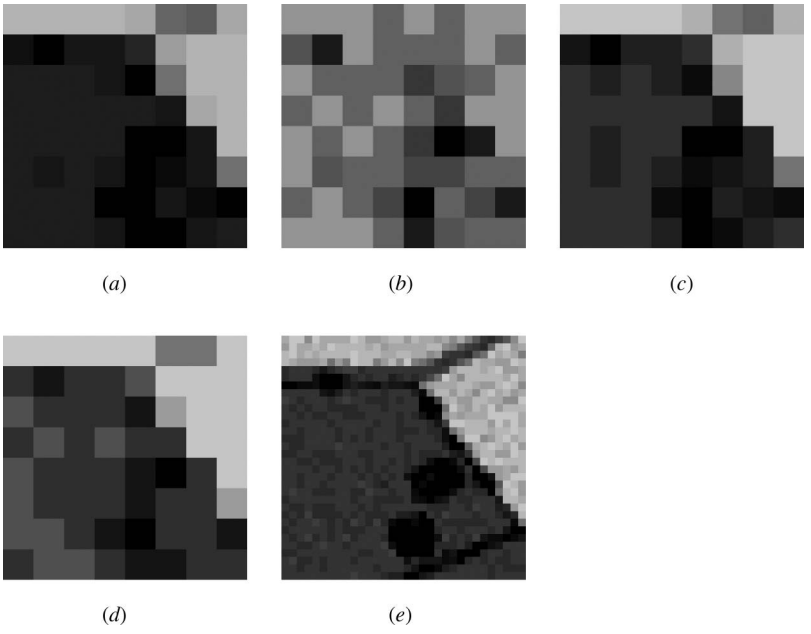

Figure 3. (*a*) Land-cover map at 4 m spatial resolution used for simulating data, (*b*) 4 m cereal class, (*c*) 4 m grass class and (*d*) 4 m trees class.

(*a*) (*b*) (*c*) (*d*)

Figure 4. Four bands ((*a*) red, (*b*) NIR, (*c*) green and (*d*) blue) of simulated MS IKONOS image with a spatial resolution of 32 m. (*e*) 8 m simulated PAN image.

image and the original MS image as in Nguyen *et al.* (2006). The end-member spectra values of the pixel (m, n) of a given 8 m MS band can be defined based on the class proportions and the reflectance values of the corresponding pixel (x, y) and its eight surrounding pixels of the same MS band at 32 m as

$$\boldsymbol{S}_{Bi} = (\boldsymbol{P}^T\boldsymbol{P})^{-1}\boldsymbol{P}^T\boldsymbol{R}_{Bi}, \tag{17}$$

where $\boldsymbol{S}_{Bi}^{xy} = [S_{BiC1} \ldots S_{BiCc}]$ and S_{BiCj} is the end-member spectra value of class C_j in spectral band B_i, $\boldsymbol{R}_{Bi} = [R_{Bi}^{(x-1)(y-1)} \ldots R_{Bi}^{(x+1)(y+1)}]^T$ is the vector of reflectance values where R_{Bi}^{xy} is the reflectance value of pixel (x, y) for spectral band B_i and

$$\boldsymbol{P} = \begin{bmatrix} P_{C1}^{(x-1)(y-1)} & \cdots & P_{Cc}^{(x-1)(y-1)} \\ \cdots & \cdots & \cdots \\ P_{C1}^{xy} & \cdots & P_{Cc}^{xy} \\ \cdots & \cdots & \cdots \\ P_{C1}^{(x+1)(y+1)} & \cdots & P_{Cc}^{(x+1)(y+1)} \end{bmatrix}, \tag{18}$$

where P_{Cj}^{xy} is the proportion value of pixel (x, y) for class C_j.

Amongst the pixels that are used to determine the local end-member spectra, the pixel (x, y) should be the most important since it covers the PAN pixel (m, n). To emphasise the contribution of the corresponding pixel (x, y) to the end-member spectra, a weight mechanism was used such that equation (17) becomes

$$\boldsymbol{S}_{Bi} = (\boldsymbol{P}^T\mathbf{W}\boldsymbol{P})^{-1}\mathbf{W}\boldsymbol{P}^T\boldsymbol{R}_{Bi}, \tag{19}$$

where $\mathbf{W}$ is the diagonal matrix:

$$\mathbf{W} = \begin{bmatrix} w^{(x-1)(y-1)} & 0 & 0 & 0 & 0 \\ 0 & \ldots & 0 & 0 & 0 \\ 0 & 0 & w^{xy} & 0 & 0 \\ 0 & 0 & 0 & \ldots & 0 \\ 0 & 0 & 0 & 0 & w^{(x+1)(y+1)} \end{bmatrix}. \tag{20}$$

and $w^{(x-1)(y-1)}, \ldots, w^{xy}, \ldots, w^{(x+1)(y+1)}$ are weight values for each corresponding pixel. The optimal weight value w^{xy} was tested using weights w^{xy} of 1 to 20 and other weight values of 1.

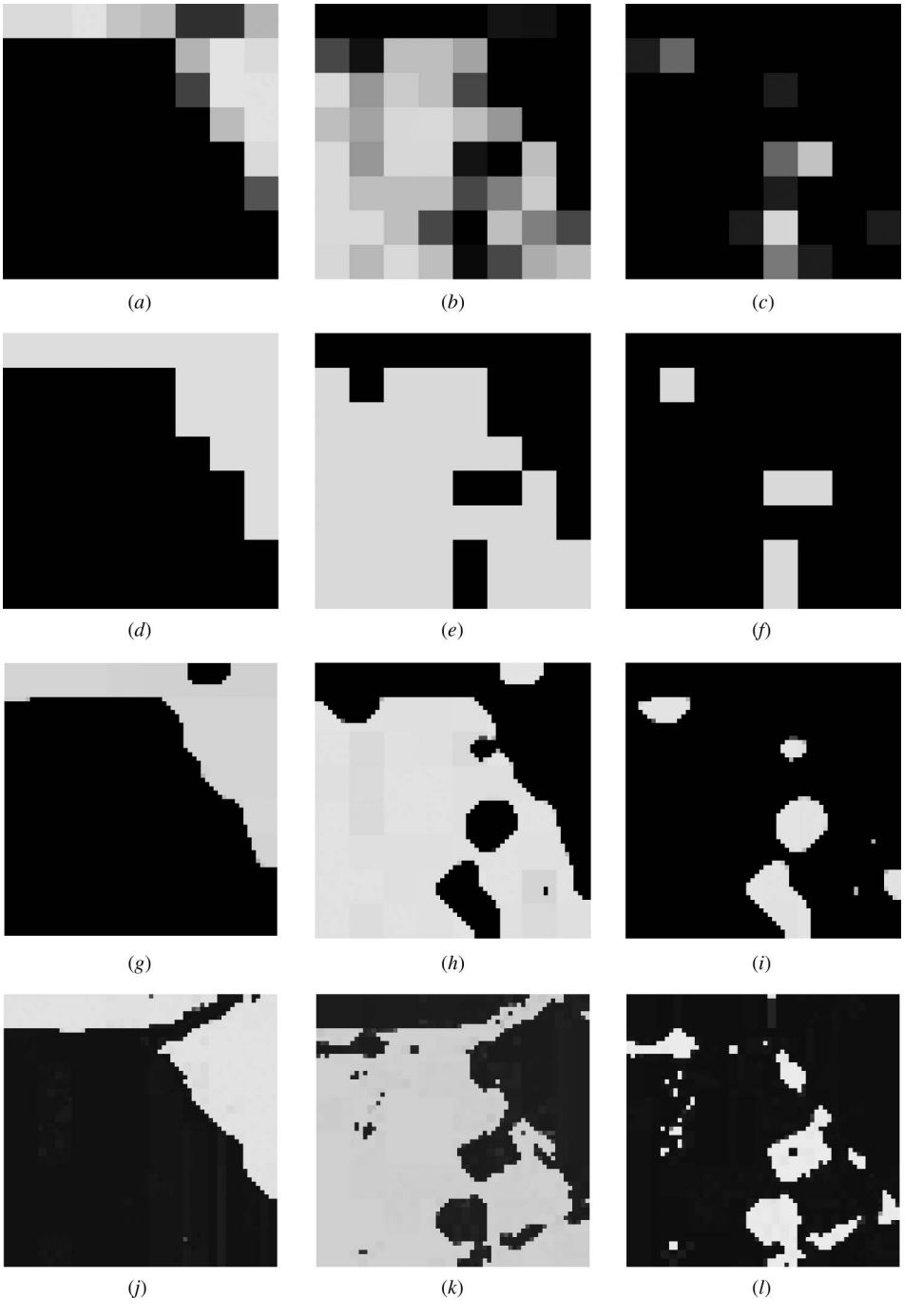

Figure 5. Land-cover proportion images with a spatial resolution of 32 m for (*a*) cereal, (*b*) grass and (*c*) trees. Hard-classified land-cover image with a spatial resolution of 32 m for (*d*) cereal, (*e*) grass and (*f*) trees. HNN super-resolution mapping image with a spatial resolution of 4 m for (*g*) cereal, (*h*) grass and (*i*) trees. HNN super-resolution mapping with PAN image with a spatial resolution of 4 m for (*j*) cereal, (*k*) grass and (*l*) trees.

3.3 *Local spectral convolution weighting factor*

As for the end-member spectra, the spectral convolution weighting factors can be determined locally using the least square method. The spectral convolution weighting factors of a pixel (m, n) of the PAN image were calculated based on the digital value of the MS and PAN pixels, which are covered by the corresponding pixel (x, y), and eight surrounding pixels at the MS image spatial resolution.

$$\boldsymbol{\Phi}^{mn} = (\boldsymbol{R}_{MS}^{T}\boldsymbol{R}_{MS})^{-1}\boldsymbol{R}_{MS}^{T}\boldsymbol{R}_{\mathrm{Pan}} \tag{21}$$

where $\boldsymbol{\Phi}^{yx}\begin{bmatrix}\varphi_{B1}\\ \dots\\ \varphi_{Bb}\end{bmatrix}$, $\boldsymbol{R}_{MS} = \begin{bmatrix} R_{B1}^{(x-1)(y-1)} & \dots & R_{Bb}^{(x-1)(y-1)} \\ \dots & \dots & \dots \\ R_{B1}^{(x+1)(y+1)} & \dots & R_{Bb}^{(x+1)(y+1)} \end{bmatrix}$, $\boldsymbol{R}_{\mathrm{Pan}} = \begin{bmatrix} R_{\mathrm{Pan}}^{(x-1)(y-1)} \\ \dots \\ R_{\mathrm{Pan}}^{(x+1)(y+1)} \end{bmatrix}$, R_{Bi}^{xy} is the digital value of the pixel (x, y) of the MS band B_i and R_{Pan}^{xy} is the digital value of the pixel (x, y) of the PAN band.

3.4 *Results*

Using the 32 m soft-classified land-cover proportions image (figure 5(*a*)–(*c*)), 4 m sub-pixel land-cover maps were obtained using the traditional HNN (figure 5(*g*)–(*i*)) and the HNN using the PAN image with local end-member spectra (figure 5(*j*)–(*l*)). The greatest accuracy land-cover map was obtained with weighting coefficients of $k_1 = 100$, $k_2 = 100$, $k_3 = 100$, $k_4 = 150$ and $k_5 = 100$ after 1000 iterations. The 32 m hard-classified land-cover image (figure 5(*d*)–(*f*)) was produced from the 32 m soft-classified proportion image (figure 5(*a*)–(*c*)) by assigning a land-cover class to a given pixel based on the largest proportion. To evaluate the resulting hard land-cover maps at the sub-pixel spatial resolution of 4 m, accuracy statistics that are usually applied for hard classification based on the error matrix were used such as the Kappa Index Agreement (KIA) value – κ, overall accuracy and per-class omission and commission errors (table 1).

Comparing the results of the two prediction techniques visually, it is clear that super-resolution mapping using the PAN image is preferable to hard classification and traditional HNN super-resolution mapping. The improvement of the technique is most obviously seen in the trees class, where most of the trees objects are smaller than the 32 m simulated image pixel. Without information from the PAN image, the trees class sub-pixels of the linear objects in the bottom-right and in the top of figure 4(*c*) were clustered into larger objects to satisfy the goal functions as in figure 5(*i*). The PAN reflectance constraint produced a value to retain the reflectance for the neurons in those linear objects. Therefore, objects smaller than an original MS pixel can be mapped (figure 5(*l*)).

The accuracy statistics (table 1) showed a considerable increase in accuracy for the new technique. Overall accuracy of the land-cover map increased by around 5% from 86.52% for the hard classification to 91.02% for the super-resolution mapping using the PAN image with local spectra. The KIA value – κ increased from 0.7530 for the hard-classified map to 0.8361 for the new HNN super-resolution mapping with the PAN image. In comparison with the HNN super-resolution mapping without using the PAN image, the accuracy of the thematic map increased 2.5% in terms of overall accuracy.

Table 1. Accuracy statistics for simulated image test.

	Cereal	Grass	Tree	ErrorO (%)	ErrorC (%)
Statistics for the hard-classified image					
Unclassified	0	0	0		
Cereal	1005	126	21	3.74	12.76
Grass	39	2305	280	8.42	12.16
Trees	0	86	234	56.26	26.88
	KIA – $\kappa = 0.7430$			Overall accuracy = 86.52%	
Statistics for the HNN super-resolution mapping with using the PAN image					
Unclassified	0	4	3		1.000
Cereal	977	89	2	4.60	8.52
Grass	63	2350	231	8.14	11.12
Trees	4	74	299	36.82	20.69
	KIA – $\kappa = 0.7814$			Overall accuracy = 88.53%	
Statistics for the HNN super-resolution mapping without using the PAN image					
Unclassified	10	70	31		1.000
Cereal	983	30	2	5.84	3.15
Grass	34	2349	106	6.67	5.62
Trees	17	68	396	25.98	17.67
	KIA – $\kappa = 0.8361$			Overall accuracy = 91.02%	

Amongst the three land-cover classes, the accuracy of the trees land-cover class increased most with the omission error reduced from 56.26% for the hard-classified image and 36.82% for the traditional HNN super-resolution mapping to approximately 25% for the new HNN super-resolution mapping technique. Similarly, the commission error reduced from 26.25% and 20.69% to 17.67% after using the PAN image. In the other two classes, the increase in accuracy was not as great as that of the trees class, since most sub-pixels in these two classes were grouped into objects larger than a 32 m pixel. However, the increase in values is relatively large if the low omission and commission errors are taken into account. This can be explained by the fact that the clustering goal functions are suitable for large features, yet the detailed information at the fused spatial resolution is essential for more accurate super-resolution mapping of the boundary pixels.

The number of unclassified pixels (table 1) was increased slightly in the super-resolved land-cover image using the PAN image in comparison with the results of the traditional HNN super-resolution mapping. These unclassified sub-pixels occurred, as the goal functions, proportion constraint and multi-class constraint could not be satisfied simultaneously. However, the number of unclassified pixels did not reduce the accuracy of the new technique.

4. Example 2: degraded QuickBird image

To provide a more realistic test of the new algorithm, a second set of proportion images was produced using degraded QuickBird MS and PAN images. The degraded QuickBird MS and PAN images are similar to the real QuickBird MS and PAN images. Furthermore, with the degraded QuickBird MS and PAN images, it is possible to evaluate directly the impact of the image registration error on the new algorithms because the land-cover classes at the sub-pixel level are known. For the degraded

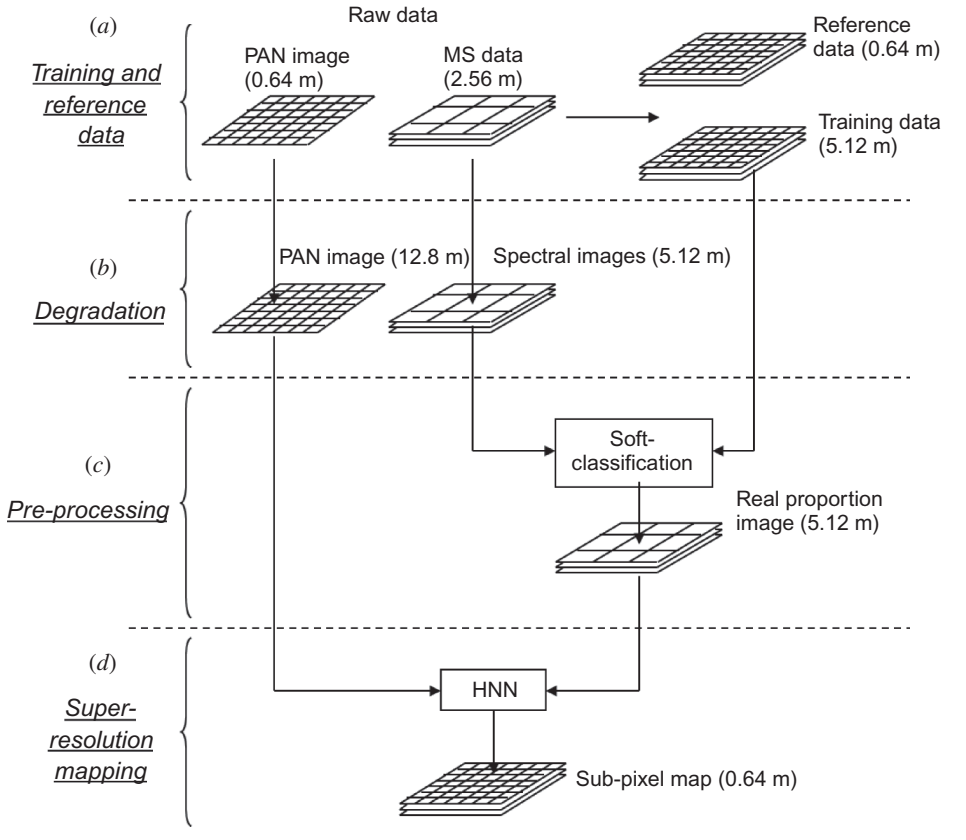

Figure 6. Four steps in the experiments: (*a*) raw data analysis, (*b*) data simulation, (*c*) preprocessing and (*d*) super-resolution mapping.

QuickBird image, the experiment was implemented in four steps: (1) training and reference data, (2) degradation, (3) preprocessing and (4) super-resolution mapping (figure 6).

4.1 *Training and reference data*

A QuickBird MS image was acquired over an area of Christchurch, UK, on 1 June 2002. Two sub-areas were extracted from images of rural landscape to test the algorithm. The first area was covered by 328×296 pixels of a 0.64 m PAN image (figure 7(*a*)) and 82×74 pixels of a 2.56 m MS image (figure 7(*b*)–(*e*)). There are four land-cover classes in the area: green cereal, grass, asphalt and white cereal. These images were used to test the performance of the new algorithm in relation to linear features such as an asphalt surface road. The second area was covered by 336×352 pixels of a 0.64 m PAN image (figure 7(*f*)) and 84×88 pixels of a 2.56 m MS image (figure 7(*g*)–(*j*)). This area contains six land-cover classes: houses (two types), trees, asphalt, grass and shadow. Therefore, it is possible to evaluate the new algorithm in terms of its ability to reconstruct both small and linear features. In this image, the houses are divided into two classes – house 1 and house 2 – based on the material of the roofs. In both areas, the MS image was co-registered to the PAN image with a RMS error of 0.25 pixels.

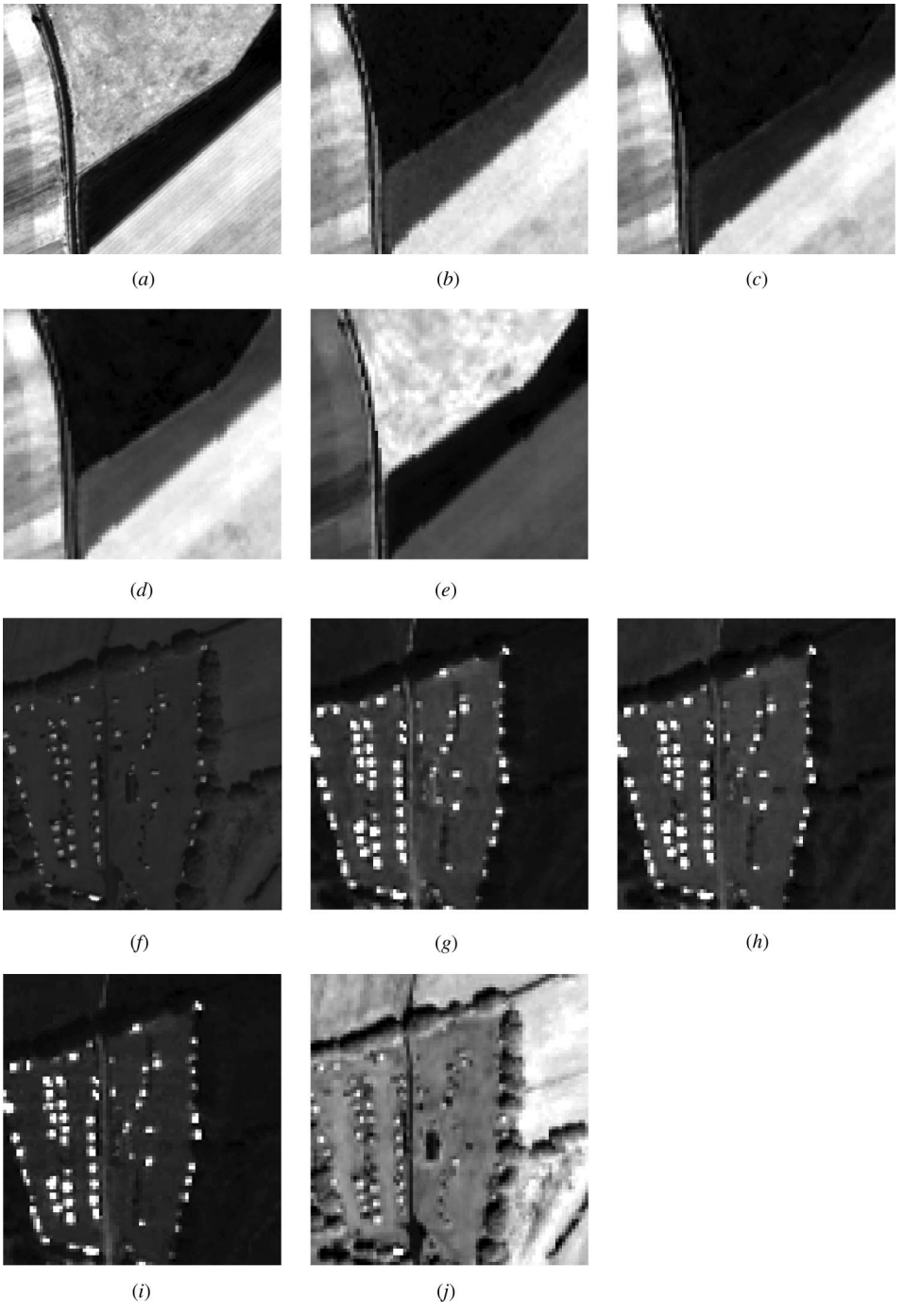

Figure 7. Study site 1: (*a*) 0.64 m PAN image (328 × 296 pixels). (*b*) blue, (*c*) green, (*d*) red and (*e*) NIR bands of 2.56 m MS image (82 × 74 pixels). Study site 2: (*f*) 0.64 m PAN image (336 × 352 pixels). (*g*) blue, (*h*) green, (*i*) red and (*j*) NIR bands of 2.56 m MS image (84 × 88 pixels).

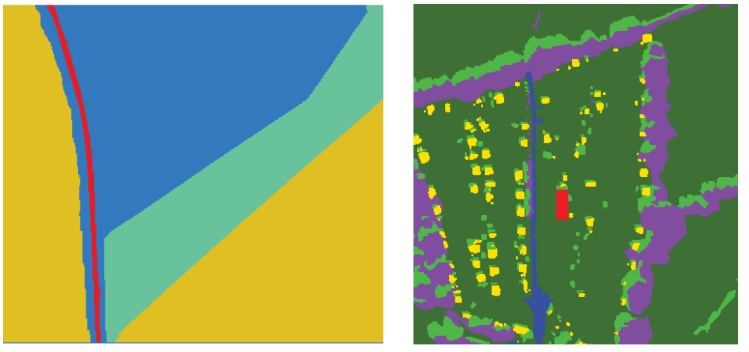

(*a*) (*b*)

Figure 8. (*a*) Four reference land-cover classes at 0.64 m spatial resolution for test site 1: yellow, white cereal; cyan, green cereal; red, asphalt road; light blue, grass. (*b*) Six reference land-cover classes at 0.64 m spatial resolution for test site 2: yellow, house 1; red, house 2; blue, asphalt road; green, grass; purple, tree; and light green, shadow.

The land-cover classes (at 0.64 m spatial resolution) of both areas were obtained by manual digitizing from the PAN image (figure 8(*a*) and (*b*)). These land-cover images were used as the reference data for the results of super-resolution mapping. Thus there was no image registration error of the PAN image against the reference data.

Super-resolution methods use land-cover proportions obtained by soft classification as input. To implement the soft classification, training data are required. In this article, the soft classification was implemented at 5.12 m spatial resolution. The training data, therefore, could be produced by degrading the land-cover image at 0.64 m spatial resolution by eight times.

4.2 *Data degradation*

The QuickBird MS images of test site 1 and test site 2 at 2.56 m spatial resolution were degraded by two times to produce MS images at 5.12 m spatial resolution of test site 1 (figure 9(*a*)–(*d*)) and test site 2 (figure 9(*i*)–(*l*)). These MS images were then used to produce the land-cover proportions at 5.12 m spatial resolution using soft classification. The land-cover proportions were then used to produce a 0.64 m land-cover image using super-resolution mapping and the results were compared with the reference data in figure 8.

The 1.28 m PAN image was degraded from the 0.64 m PAN image by two times (figure 9(*e*) and (*m*)). The PAN image in figure 9(*e*) and (*m*) contained no image registration error. To evaluate the effect of the image registration error on the accuracy of the resulting land-cover map, the PAN image was geo-coded with a RMS of 0.5 pixels (figure 9(*f*) and (*n*)), 1 pixel (figure 9(*g*) and (*o*)) and 1.5 pixels (figure 9(*h*)). The proposed algorithm was then tested using these geo-coded PAN images, and the results were compared with those of the PAN images without image registration error.

4.3 *Preprocessing*

Proportion images at 5.12 m spatial resolution were produced from the 5.12 m MS image in figure 9. Obviously, this set of proportion images contains a certain amount of

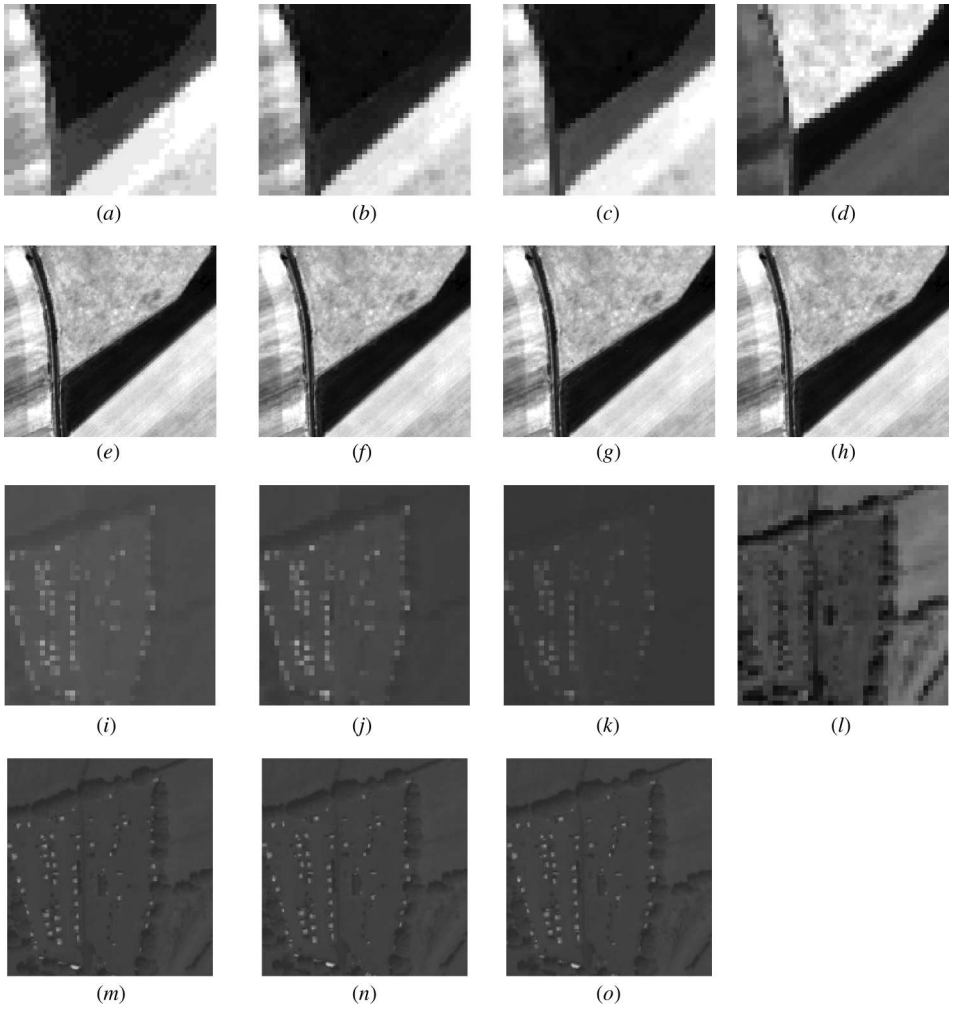

Figure 9. Four bands ((*a*) blue, (*b*) green, (*c*) red and (*d*) NIR) of simulated 5.12 m MS image of test site 1. (*e*) 1.28 m degraded PAN image, (*f*) 0.5 pixel image registration error PAN image at 1.28 m spatial resolution, (*g*) 1 pixel image registration error PAN image at 1.28 m spatial resolution and 1.5 pixel image registration error PAN image at 1.28 m spatial resolution. Four bands ((*i*) blue, (*j*) green, (*k*) red and (*l*) NIR) of simulated 5.12 m MS image of test site 2. (*m*) 1.28 m degraded PAN image, (*n*) 0.5 pixel image registration error PAN image at 1.28 m spatial resolution and (*o*) 1 pixel image registration error PAN image at 1.28 m spatial resolution.

error, including the MS image registration error. The predicted land-cover proportions were then used for hard classification, traditional super-resolution mapping and the new method for super-resolution mapping using the PAN image. This means that the results of all these methods were affected by the same amount of error contained in the land-cover proportions. The only difference between the new method of super-resolution mapping and the other methods is that the results of this method were also affected by the registration error of the PAN image. Therefore, it is necessary to evaluate the impact of the PAN image registration error on the methods.

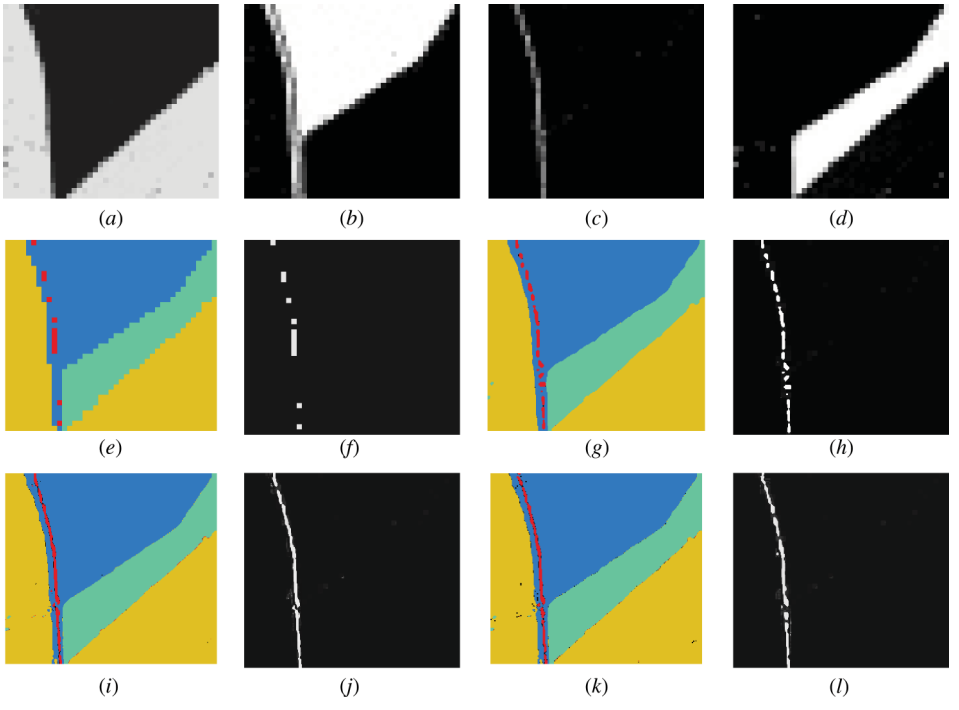

Figure 10. (*a*) White cereal, (*b*) grass, (*c*) asphalt and (*d*) green cereal 5.12 m land-cover proportion images. (*e*) 5.12 m hard-classified land-cover image, (*f*) 5.12 m hard-classified asphalt land-cover class. (*g*) 0.64 m HNN super-resolution mapping image, (*h*) 0.64 m HNN super-resolution mapping asphalt land-cover class. (*i*) 0.64 m HNN super-resolution mapping using the PAN without image registration error and (*j*) 0.64 m asphalt land-cover class obtained by HNN super-resolution mapping using the PAN without image registration error. (*k*) 0.64 m HNN super-resolution mapping using the PAN image with RMS image registration error of 1 pixel and (*l*) 0.64 m asphalt land-cover class obtained by HNN super-resolution mapping using the PAN image with RMS image registration error of 1 pixel.

A k-NN was used for soft classification with $k = 5$. The land-cover proportion images were produced with an overall area error proportion of $P = 0.032\%$ and an overall RMS error of 0.0332 pixels for test site 1. The predicted proportions of four land-cover classes in test site 1 can be seen in figure 10(*a*)–(*d*). In test site 2, the land-cover proportions were predicted with an overall area error proportion of $P = 0.079\%$ and an overall RMS error of 0.103 pixels (figure 11).

4.4 *Super-resolution mapping – results*

To evaluate the performance of the new algorithms with degraded QuickBird imagery, the results for test site 1 and test site 2 produced by the three approaches were compared visually and statistically, as in the simulated data case. The 5.12 m hard-classified land-cover map was obtained from the land-cover proportion image by assigning each 5.12 m pixel to the class of the largest proportion, as shown in figure 10(*e*) for test site 1 and figure 12(*d*) for test site 2. Applying the traditional HNN super-resolution mapping approach (Tatem *et al.* 2001a), a 0.64 m spatial resolution land-cover map was

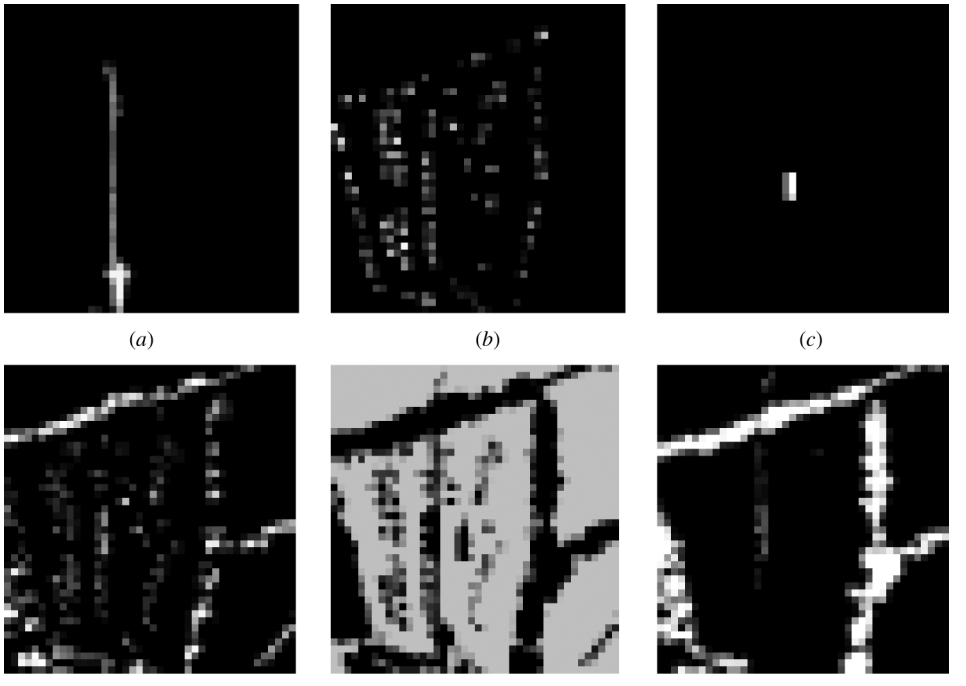

Figure 11. Land-cover proportion images with a spatial resolution of 5.12 m for (*a*) asphalt, (*b*) house 1, (*c*) house 2, (*d*) shadow, (*e*) grass and (*f*) tree.

produced from the 5.12 m proportion images with a zoom factor of 8, weighting constants of $k_1 = 100$, $k_2 = 100$, $k_3 = 150$ and $k_4 = 100$ and 1000 iterations (figure 10(*g*) for test site 1 and figure 12(*g*) for test site 2).

The new HNN super-resolution mapping technique was tested with the 5.12 m land-cover class proportion images and the 1.28 m PAN images. With 1000 iterations, a zoom factor of 8, weighting constants of $k_1 = 100$, $k_2 = 100$, $k_3 = 150$, $k_4 = 100$ and $k_5 = 100$, the HNN network using the PAN image without registration error produced the land-cover images in figure 10(*i*) (test site 1) and 12(*j*) (test site 2). Using the same weighting constants with the PAN image with image registration RMS error of 1 pixel (an accuracy commonly obtained in the geometric correction process), the HNN produced the land-cover maps, as in figure 10(*k*) (test site 1) and figure 12(*m*) (test site 2). To evaluate the new technique statistically, the error matrix and the accuracy statistics such as the KIA value, omission, commission and overall errors for the resulting maps of the three methods are given in table 2.

The results in figure 10 show the advantage of the new technique in comparison with the hard classification and the HNN super-resolution mapping without using PAN images. In test site 1 and test site 2, similar to the simulated IKONOS data set, the greatest increase in accuracy can be seen in the asphalt class, where most sub-pixels belong to linear objects. Without information from the PAN image, the road sub-pixels in figure 8(*a*) were split into separate objects to satisfy the HNN goal functions, as in figure 10(*h*) and figure 12(*h*). With information from the PAN image, the reconstruction of the asphalt-surface road objects was improved greatly, as seen in figure 10(*j*),

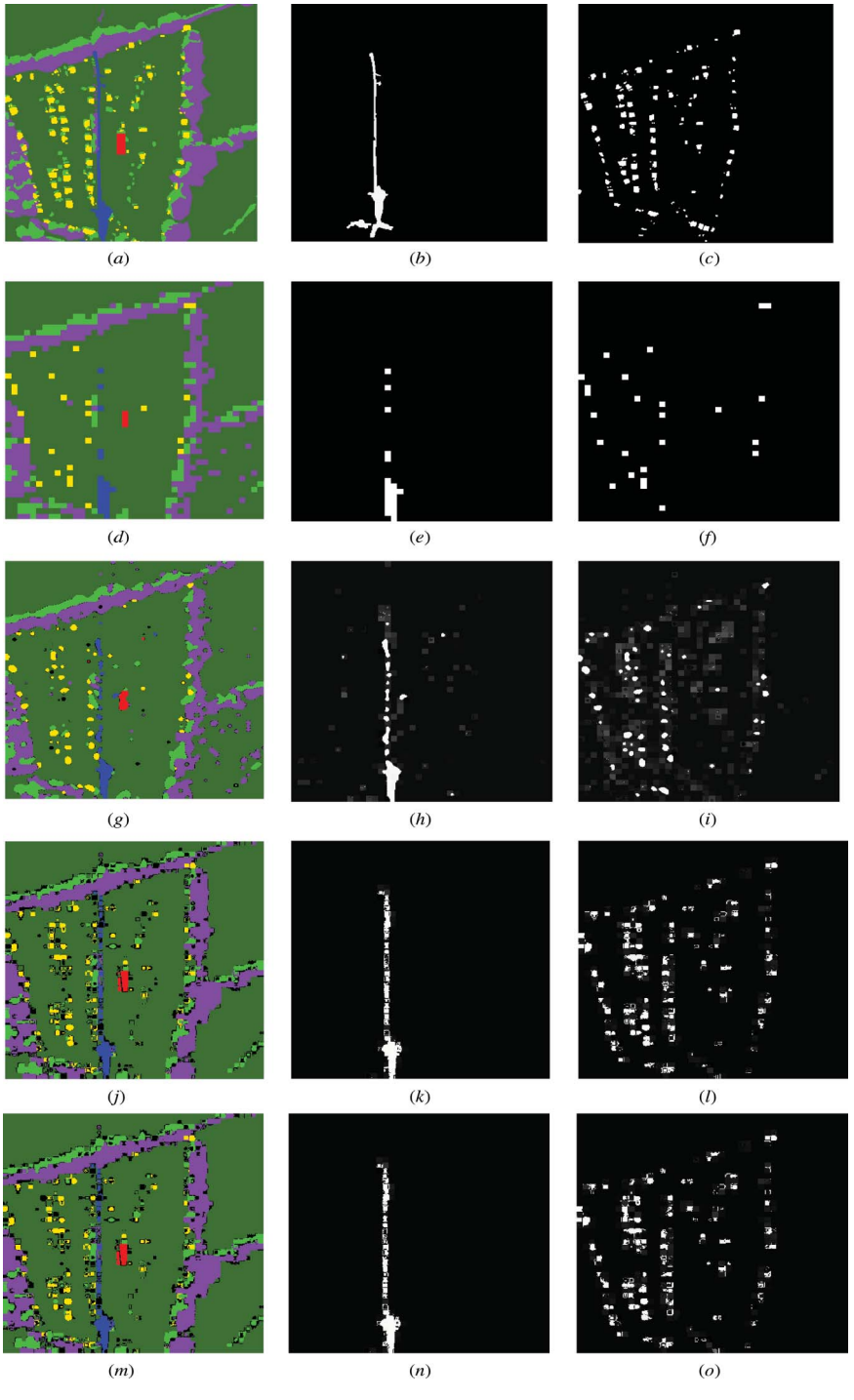

Figure 12. Reference (*a*) land-cover map, (*b*) asphalt class and (*c*) house 1 class. Hard-classified (*d*) land-cover map, (*e*) asphalt class and (*f*) house 1 class. Traditional HNN super-resolution mapping (*g*) land-cover map, (*h*) asphalt class and (*i*) house 1 class. HNN super-resolution mapping using PAN image (with no-registration error) (*j*) land-cover map, (*k*) asphalt class and (*l*) house 1 class. HNN super-resolution mapping (with 1 pixel registration error) (*m*) land-cover map, (*n*) asphalt class and (*o*) house 1 class.

Table 2. Accuracy statistics of degraded QuickBird results – test site 1.

	W. cereal	Grass	Asphalt	G. cereal	ErrorO (%)	ErrorC (%)
Statistics for hard classification						
Unclassified	0	0	0	0	0	0
W. Cereal	41914	273	0	501	1.45	1.81
Grass	362	33776	935	191	3.31	4.22
Asphalt	0	305	463	0	39.71	66.88
G. Cereal	253	578	0	17537	4.52	3.80
KIA – $\kappa = 0.9454$				Overall accuracy = 96.50%		
Statistics for traditional HNN super-resolution mapping image						
Unclassified	0	5	5	1	0	1.00
W. Cereal	42397	123	0	295	0.31	0.98
Grass	54	34336	612	64	1.71	2.08
Asphalt	1	298	781	0	27.69	44.13
G. Cereal	77	170	0	17869	1.97	1.36
KIA – $\kappa = 0.9726$				Overall accuracy = 98.24%		
Statistics for the new HNN super-resolution mapping using the PAN image with no registration error						
Unclassified	35	82	55	30	0	1.00
W. Cereal	42279	129	0	126	0.59	0.60
Grass	72	34408	252	30	1.50	1.02
Asphalt	1	195	1091	0	21.96	15.23
G. Cereal	142	118	0	18043	1.02	1.42
KIA – $\kappa = 0.9797$				Overall accuracy = 98.69%		
Statistics for the new HNN super-resolution mapping using the PAN image with registration error of 1 pixel						
Unclassified	42	92	57	32	0	1.00
W. Cereal	42234	53	0	131	0.69	0.44
Grass	111	34391	343	24	1.55	1.37
Asphalt	0	223	998	0	28.61	18.26
G. Cereal	142	173	0	18041	1.03	1.72
KIA – $\kappa = 0.9772$				Overall accuracy = 98.53%		

Note: W. cereal, white cereal; G. cereal, green cereal.

figure 10(*l*) and figure 12(*k*) and (*n*). Even when the PAN image was registered with an RMS error of 1 pixel, the linear road object was still more contiguous than that of the HNN super-resolution mapping without using the PAN data.

The increased accuracy of the new algorithm on small objects can also be seen in the house 1 class in test site 2. House objects, which can be seen in figure 12(*c*), mostly disappeared in the hard classification in figure 12(*g*) and sometimes were lost in super-resolution without PAN data, but were reproduced in figure 12(*l*) and figure 12(*o*). This fact suggests that the new technique is applicable for the identification of small targets.

The advantage of the new technique was also demonstrated by the accuracy statistics. In test site 1, the overall accuracy of the land-cover map increased by around 2% from 96.50% for the hard classification to 98.69% for the super-resolution mapping using the PAN image without image registration error. With the PAN image with image registration error of 1 pixel, the accuracy of the resulting 0.64 m land-cover map increased around 2% and 0.45% in comparison with the results of hard classification and the HNN super-resolution mapping technique respectively. The KIA value

increased from 0.9454 for the hard-classified map and 0.9726 for the traditional HNN sub-pixel map to 0.9797 for the super-resolution mapping using PAN image without registration error and 0.9772 for the super-resolution mapping using PAN image with registration error of 1 pixel. In test site 2, the increase in the accuracy is shown in KIA, which increased from 0.6696 for the traditional HNN super-resolution mapping technique to 0.6966 and 0.6960 for the new algorithms with no registration error PAN and 1 pixel registration error PAN, respectively.

The accuracy statistics also demonstrated that amongst the land-cover classes, the accuracy of the classes with small and linear objects increased most. For the asphalt class in test site 1, omission error decreased from 39.71% for the hard-classified image and 27.69% for the traditional HNN super-resolution mapping to 21.96% for the new HNN super-resolution mapping technique using the PAN image without registration error. Although the omission error for the new method increased slightly from 27.69% for the traditional HNN super-resolution mapping to 28.61% due to the impact of the PAN image registration error of 1 pixel, the commission error reduced from 66.88% for the hard classification and 44.13% for the HNN to 18.26%. For the other two classes in test site 1, where most sub-pixels were grouped into larger objects, the increase in accuracy of the other two classes was not as great as that of the asphalt class. The decreases in the commission and omission errors were around 1%. However, it is still a considerable increase in accuracy if the very high starting accuracies of these classes are taken into account.

As for test site 1, the increase in accuracy for the newly proposed algorithm compared with the traditional HNN super-resolution mapping for test site 2 is seen mostly in the asphalt and house 1 classes, which contain linear and small objects (table 3). For these two classes, the omission error decreased by 8% and 7%, respectively, whereas the commission error for the asphalt class decreased by 6.3%. The only decrease in accuracy is seen in the increase of commission error of 3% for the house 1 class. However, for test site 2, the increase in accuracy is not clearly observed for large objects such as grass, tree or shadow. There was an increase in accuracy for the tree and shadow classes with an increase of around 8% in the omission error from 26.73% to 18.94% for the tree class, but the omission error for grass rose by 2% from 4.34% to 6.88%.

The experiment on test site 2 showed that the new algorithm can work with a large number of classes. The new method in this article has some similarities with that presented in Nguyen *et al.* (2006). However, the algorithm for super-resolution mapping with fused images is only applicable to sites where the number of classes is smaller than the number of bands in the MS image. In test site 2, the number of classes is six, whereas the number of spectral bands is only four. Using reflectance minimum difference comparison, the newly proposed method can be used for sites with a large number of classes.

4.5 *Conflicts between the goal and constraint functions*

Although the accuracy of the new method increased in comparison with other methods, there exists a problem of conflict between the goal and constraints functions of the HNN. In the traditional HNN for super-resolution mapping, the outputs of neurons have to satisfy both goal functions, proportion constraint and multi-class constraint (equation (5)), and the last outputs of neurons have to approach the value of 1 or 0. This means that there are only a few cases where two neurons at the same geographical

Table 3. Accuracy statistics of degraded QuickBird results – test site 2.

	Asphalt	House 1	House 2	Shadow	Trees	Grass	ErrorO (%)	ErrorC (%)
Statistics for hard classification								
Unclassified	0	0	0	0	0	0	0	0
Asphalt	914	2	0	33	38	293	0.5022	0.2859
House 1	0	960	0	181	83	376	0.7634	0.4000
House 2	0	0	192	0	0	0	0.4839	0.0000
Shadow	0	222	0	4580	1066	788	0.5495	0.3119
Trees	46	121	0	1909	12521	1787	0.3005	0.2358
Grass	876	2752	180	3463	4192	80697	0.0386	0.1244
KIA – $\kappa = 0.6299$				Overall accuracy = 84.44%				
Statistics for traditional HNN super-resolution mapping image								
Unclassified	60	166	9	354	445	685	0	1.0000
Asphalt	975	27	0	17	66	314	0.4690	0.3031
House 1	0	1263	0	187	44	386	0.6887	0.3282
House 2	0	2	293	0	0	20	0.2124	0.0698
Shadow	8	226	1	5283	899	664	0.4803	0.2539
Trees	34	98	0	1570	13116	1576	0.2673	0.2000
Grass	759	2275	69	2755	3330	80276	0.0434	0.1027
KIA – $\kappa = 0.6696$				Overall accuracy = 85.59%				
Statistics for the new HNN super-resolution mapping without PAN image registration error								
Unclassified	397	1053	49	2131	1925	3638	0.0000	1.0000
Asphalt	1129	0	0	25	91	242	0.3851	0.2408
House 1	0	1579	0	248	101	543	0.6108	0.3610
House 2	0	0	304	0	0	41	0.1828	0.1188
Shadow	6	244	0	5259	677	762	0.4827	0.2431
Trees	99	102	0	823	14506	549	0.1896	0.0978
Grass	205	1079	19	1680	600	78166	0.0688	0.0438
KIA – $\kappa = 0.6966$				Overall accuracy = 85.35%				
Statistics for the new HNN super-resolution mapping with PAN image registration error of 1 pixel								
Unclassified	405	1040	49	2159	1919	3650	0.0000	1.0000
Asphalt	1129	0	0	28	87	243	0.3851	0.2408
House 1	0	1573	0	249	102	540	0.6123	0.3616
House 2	0	0	304	0	0	41	0.1828	0.1188
Shadow	4	240	0	5233	676	754	0.4852	0.2424
Trees	91	98	0	821	14509	543	0.1894	0.0967
Grass	207	1106	19	1676	607	78170	0.0688	0.0442
KIA – $\kappa = 0.6960$				Overall accuracy = 85.33%				

position have values that are >0.5. However, in the new algorithm, the addition of the new PAN reflectance constraint may prevent satisfaction of the multi-class constraint and there may exist neurons of different classes in the same position with output values >0.5 at the point that the HNN is stopped. In the accuracy assessment in table 2, these neurons were labelled as unclassified and presented in black in the resulting land-cover maps in figure 12(*j*) and (*m*).

Accuracy statistics for test site 2 in table 3 showed that the number of unclassified sub-pixels increased greatly by adding the PAN reflectance constraint. In the traditional HNN super-resolution mapping, the total number of unclassified sub-pixels is only 1719, whereas the number of unclassified sub-pixels in new HNN super-resolution mapping using PAN image is 9193 without registration error and 9222 with registration error of 1 pixel.

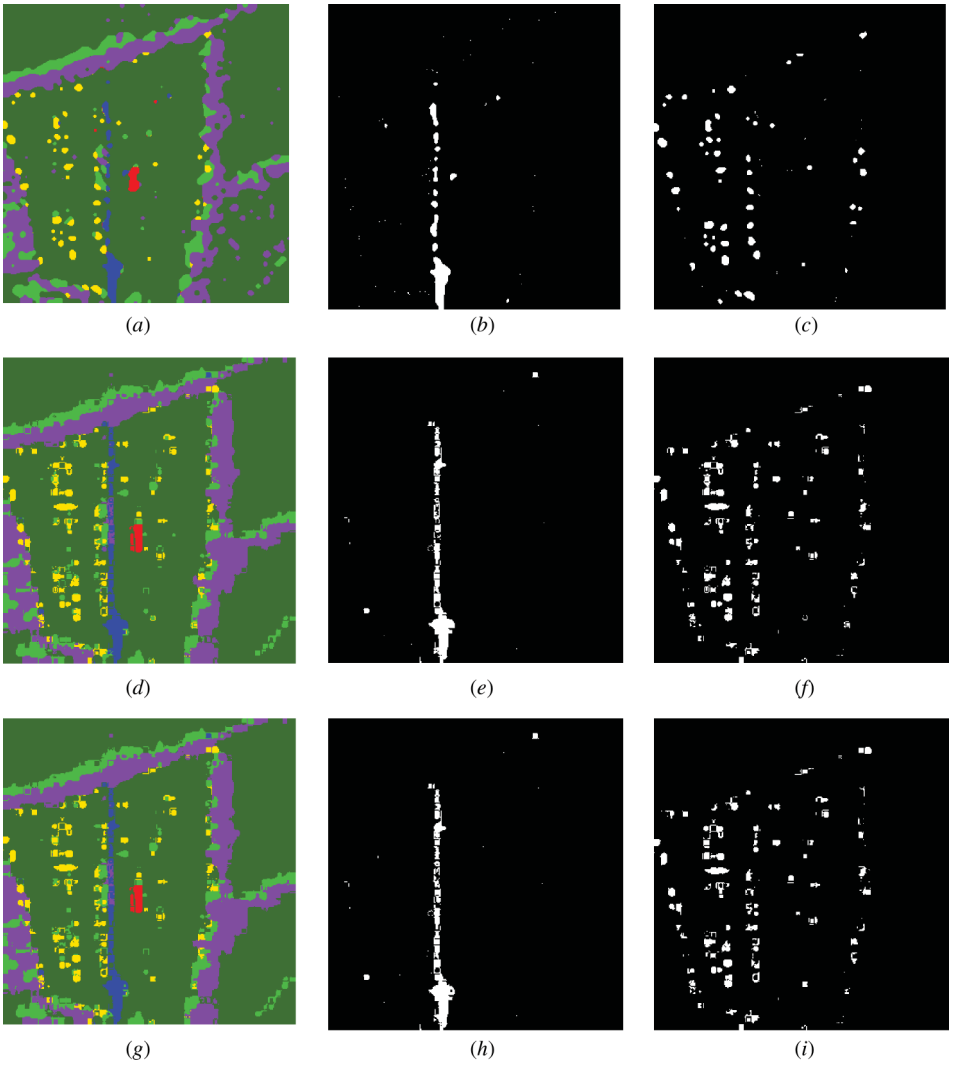

Figure 13. Land-cover maps from HNN super-resolution mapping with maximization rule. Traditional HNN super-resolution mapping results: (*a*) land-cover map, (*b*) asphalt class and (*c*) house 1 class. HNN super-resolution mapping (with no-registration error) PAN maximization results: (*d*) land-cover map, (*e*) asphalt class and (*f*) house 1 class. Traditional HNN super-resolution mapping (with 1 pixel registration error) maximization results: (*g*) land-cover map, (*h*) asphalt class and (*i*) house 1 class.

To resolve this problem, a simple maximization rule was used to assign a sub-pixel to a land-cover class based on the largest value of neuron output. For example, if the output value of a neuron representing the asphalt class at the position (m, n) is 0.8 and the output value of the neuron representing the tree class at the same position is 0.9, then the sub-pixel at the position (m, n) will be assigned to the tree class. Using this rule, the results of super-resolution mapping are shown in figure 13, and the corresponding accuracy statistics are given in table 4. The statistics show that the accuracy

Table 4. Accuracy statistics of degraded QuickBird results – test site 2, maximization rule.

	Asphalt	House 1	House 2	Shadow	Trees	Grass	ErrorO (%)	ErrorC (%)
Statistics for traditional HNN super-resolution mapping image								
Asphalt	994	38	0	32	80	342	0.4586	0.3311
House 1	2	1327	0	208	59	471	0.6729	0.3580
House 2	6	8	297	6	6	34	0.2016	0.1681
Shadow	9	239	0	5412	966	742	0.4676	0.2655
Trees	37	109	1	1658	13337	1682	0.2549	0.2073
Grass	788	2336	74	2850	3452	80670	0.0390	0.1054
KIA – $\kappa = 0.6817$				Overall accuracy = 86.27%				
Statistics for the new HNN super-resolution mapping without PAN image registration error								
Asphalt	1410	11	0	70	127	427	0.2369	0.3119
House 1	8	2035	0	383	169	895	0.4984	0.4169
House 2	0	0	319	0	0	49	0.1425	0.1332
Shadow	10	400	0	6331	1033	1264	0.3772	0.2995
Trees	143	174	0	1145	15691	881	0.1234	0.1299
Grass	274	1437	53	2237	880	85306	0.0419	0.0572
KIA – $\kappa = 0.7768$				Overall accuracy = 89.79%				
Statistics for the new HNN super-resolution mapping with PAN image registration error of 1 pixel								
Asphalt	1419	12	0	68	130	434	0.2271	0.3122
House 1	8	2050	0	382	179	897	0.4947	0.4170
House 2	0	0	319	0	0	49	0.1425	0.1332
Shadow	17	379	0	6382	1088	1249	0.3722	0.2998
Trees	120	150	0	1094	15558	780	0.1308	0.1211
Grass	272	1466	53	2240	945	80532	0.0406	0.0582
KIA – $\kappa = 0.7774$				Overall accuracy = 89.84%				

increased greatly for HNN super-resolution mapping using the PAN image with the KIA value increased from 0.6817 to 0.7768 for no-registration error and 0.7774 for 1 pixel registration error, after the maximization rule was applied.

4.6 *Impacts of image registration error*

The impact of the PAN image registration error was determined based on variation in the KIA value as a result of an increase in the PAN image registration error. The variation is the KIA values with RMS image registration errors ranging from 0.5 to 1.5 pixels are presented in figure 14. Coherently, the plot shows that the KIA value reduced as the RMS image registration error increased. However, with a PAN image with RMS error of 1 pixel (an accuracy of image registration i.e, commonly obtained in the geometric correction of remotely sensed images), the KIA value of the sub-pixel map produced by the new method was still greater than that produced by the traditional HNN super-resolution mapping technique. When the RMS image registration error increased to 1.5 pixels, the resulting sub-pixel map predicted by the new technique was less accurate than the results of the HNN without using the PAN image. It is therefore recommended that the new technique should be used only if the PAN image is registered with an RMS error equal to or smaller than 1 pixel.

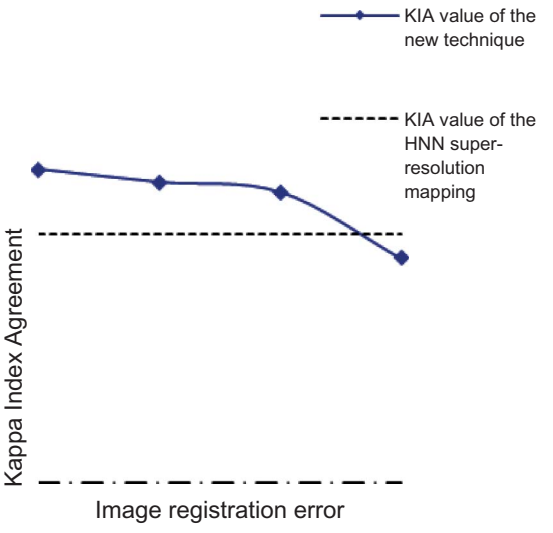

Figure 14. The effect of image registration error on the Kappa Index of Agreement value for the HNN super-resolution mapping using the PAN image.

5. Conclusion

This article introduces the use of a PAN image as supplementary data for super-resolution mapping. Information from MS and PAN images is commonly available in combination from multi-sensor remote-sensing platforms. Thus super-resolution mapping without using a PAN image can, in many cases, be seen as a disregard for available information at an intermediate spatial resolution. For that reason, this article aimed to assess the possibility of using a PAN image to increase the accuracy of super-resolution mapping.

In this article, information from PAN images was incorporated into the popular HNN super-resolution mapping approach in the form of a PAN reflectance constraint, which was added to the energy function. The value of the PAN reflectance constraint was calculated based on forward and inverse models using local end-member spectra and a local spectral convolution weighting factor. The technique was examined using both (i) a simulated IKONOS data set and (ii) a degraded QuickBird image (with and without image registration error). The accuracy of the results was evaluated based on the error matrix and accuracy statistics such as KIA value, overall accuracy and omission and commission errors.

The results from both simulated and real data sets demonstrated that PAN images can be used as a source of supplementary information for the HNN to predict land cover at a sub-pixel spatial resolution. Both the visual and statistical analysis showed that the new technique can increase the accuracy of all land-cover classes, especially for land-cover features at the sub-pixel scale. The analysis also suggests that the new technique can be applied where the RMS image registration error of the PAN image is $\leq$1 pixel. Although the new algorithm causes a conflict between the goal function and constraints, the problem can be solved by using a maximization rule.

The result of the experiments suggest the potential for using the HNN as a tool for super-resolution mapping based on a combination of PAN and MS images to produce an MS image at sub-pixel spatial resolution that is finer than either input image.

Thus future research will develop a new method using the HNN to predict MS images at the sub-pixel spatial resolution.

References

Aplin, P. and Atkinson, P.M., 2001, Sub-pixel land cover mapping for per-field classification. *International Journal of Remote Sensing*, **22**, pp. 2853–2858.

Atkinson, P.M., 1997, Mapping sub-pixel boundaries from remotely sensed images. In *Innovation in GIS 4*, Z. Kemp (Ed.), pp. 166–180 (London: Taylor & Francis).

Atkinson, P.M., 2008, Super-resolution mapping using the two-point histogram and multi-source imagery. In *geoENV VI – Geostatistics for Environmental Applications*, A. Soares, M.J. Pereira and R. Dimitrakopoulos, (Eds.), pp. 307–321 (Dordrecht: Springer).

Bastin, L., 1997, Comparison of fuzzy c-means classification, linear mixture modelling and MLC probabilities as tools for unmixing coarse pixels. *International Journal of Remote Sensing*, **18**, pp. 3629–3648.

Boucher, A. and Kyriakidis, P.C., 2006, Super-resolution land cover mapping with indicator geostatistics. *Remote Sensing of Environment*, **104**, pp. 264–282.

Brown, M., Lewis, H. and Gunn, S., 2000, Linear spectral mixture models and support vector machines for remote sensing. *IEEE Transactions on Geoscience and Remote Sensing*, **38**, pp. 2346–2360.

Carpenter, G.M., Gopal, S., Macomber, S., Martens, S. and Woodcock, C.E., 1999, A neural network method for mixture estimation for vegetation mapping. *Remote Sensing of Environment*, **70**, pp. 138–152.

Foody, G.M., 2004, Sub-pixel methods in remote sensing. In *Remote Sensing Image Analysis*, S.M. de Jong and F. van der Meer (Eds.), pp. 37–49 (Dortrecht: Kluwer Academic).

Foody, G.M., Lucas, R.M., Curran, P.J. and Honzak, M., 1997, Non-linear mixture modelling without end-members using an artificial neural network. *International Journal of Remote Sensing*, **18**, pp. 937–953.

Mertens, K.C., Verbeke, L.P.C., Ducheyne, E.I. and De Wulf, R.R., 2003, Using genetic algorithms in sub-pixel mapping. *International Journal of Remote Sensing*, **24**, pp. 4241–4247.

Mertens, K.C., Verbeke, L.P.C., Westra, T. and De Wulf, R.R., 2004, Sub-pixel mapping and sub-pixel sharpening using neural network predicted wavelet coefficients. *Remote Sensing of Environment*, **91**, pp. 225–236.

Nguyen, Q.M., Atkinson, P.M. and Lewis, H.G., 2005, Super-resolution mapping using Hopfield neural network with LiDAR data. *IEEE Geoscience and Remote Sensing Letters*, **2**, pp. 366–370.

Nguyen, Q.M., Atkinson, P.M. and Lewis, H.G., 2006, Super-resolution mapping using Hopfield neural network with fused images. *IEEE Transactions on Geoscience and Remote Sensing*, **44**, pp. 736–749.

Schowengerdt, R.A., 1996, On the estimation of spatial-spectral mixing with classifier likelihood functions. *Pattern Recognition Letters*, **17**, pp. 1379–1387.

Schowengerdt, R.A., 1997, *Remote Sensing: Models and Methods for Image Processing*, pp. 389–470 (San Diego, CA: Academic Press).

Settle, J.J. and Drake, N.A., 1993, Linear mixing and the estimation of ground cover proportions. *International Journal of Remote Sensing*, **14**, pp. 1159–1177.

Tatem, A.J., Lewis, H.G., Atkinson, P.M. and Nixon, M.S., 2001a, Super-resolution target identification from remotely sensed images using a Hopfield neural network. *IEEE Transactions on Geoscience and Remote Sensing*, **39**, pp. 781–796.

Tatem, A.J., Lewis, H.G., Atkinson, P.M. and Nixon, M.S., 2001b, Multi-class land cover mapping at the sub-pixel scale using a Hopfield neural network. *International Journal of Applied Earth Observation and Geoinformation*, **3**, pp. 184–190.

Tatem, A.J., Lewis, H.G., Atkinson, P.M. and Nixon, M.S., 2002, Super-resolution land cover pattern prediction using a Hopfield neural network. *Remote Sensing of Environment*, **79**, pp. 1–14.

Verhoeye, J. and De Wulf, R., 2002, Land cover mapping at sub-pixel scales using linear optimisation techniques. *Remote Sensing of Environment*, **79**, pp. 96–104.

Zhang, L., Wu, K., Zhong, Y. and Li, P., 2008, A new sub-pixel mapping algorithm based on a BP neural network with an observation model. *Neurocomputing*, **71**, pp. 2046–2054.

Zhang, Y., 1999, A new merging method and its spectral and spatial effects. *International Journal of Remote Sensing*, **20**, pp. 2003–2014.